

Sensitivity of STIS First-Order Medium Resolution Modes

Charles R. Proffitt
July 21, 2006

ABSTRACT

The sensitivities for STIS first-order medium resolution modes were redetermined using on-orbit observations of the standard DA white dwarfs G 191-B2B, GD 71, and GD 153. We review the procedures and assumptions used to derive the adopted throughputs, and discuss the remaining errors and uncertainties.

Introduction

Because of the much larger number of central wavelength settings, and the presumption that the low dispersion modes would be preferred when highly accurate flux measurements were needed, the flux calibration of the STIS medium resolution first order modes has been a lower priority than that of the low dispersion modes.

For the G140M and G230M gratings, observations of the standard DA white dwarf GD 71 obtained in 1997 and 1999 were used for the initial calibration. A few observations of another white dwarf standard GD 153 were also obtained in 1997. Note that the tilt of the G140M grating was changed in March 1999 to move the spectra from the upper to the lower part of the detector, and the two epochs need to be calibrated separately.

For the G230MB, G430M, and G750M gratings, the initial on-orbit calibration was done using observations of the hot subdwarf BD +75°325 obtained by programs 7094, 7656, and 7810 during 1997 and 1998. This star is not one of the primary white dwarf standards, but is instead a secondary standard which is tied to the primary standards through low-dispersion STIS observations. This procedure resulted in a reference spectrum that is of lower resolution than the medium resolution modes it is used to calibrate, and also tied the medium resolution calibration to the low resolution one.

Observations of G 191-B2B were obtained by programs 8421 and 8916 between January 2000 and April 2002 for most first order medium resolution central wavelength settings. In this report we describe how these newer data were used to redetermine the photometric throughput curves for the medium resolution gratings. In the appendix to this document we tabulate the existing observations of the white dwarf standards GD 71, G 191-B2B, and GD 153 that were used in this analysis.

These CCD observations of G 191-B2B were all done using full frame observations, with no onboard binning, and with the CCD gain set to 1 (the BD +75° 325 observations had used GAIN=4). All of the external target observations discussed here were done with the target positioned in the center of the wide 52X2 aperture.

The PHOTTAB reference tables p822207no_pht.fits (CCD modes), p822207qo_pht.fits (G230M), p822207oo_pht.fits (G140M below the repeller wire), and p822207po_pht.fits (G140M above the repeller wire), that implement these changes were delivered for use in STIS on-the-fly recalibration (OTFR) on August 2, 2005. Calibrated data obtained from the archive after this date will use the revised throughput curves.

Analysis

The absolute flux calibration of STIS is primarily based on observations of the DA white dwarf (WD) stars G 191-B2B, HZ 43, GD 153, and GD 71 (Bohlin, Colina, & Finley 1995). It is assumed that the spectral energy distributions (SEDs) of the nearly pure hydrogen atmospheres of these stars can be calculated with great precision. We will adopt the same model SEDs discussed by Bohlin & Gilliland (2004), and then find sensitivities for each grating by dividing the observed net count rate of each star by the model spectrum. In principle, the theoretical spectrum should be first convolved with the effects of the instrumental line-spread function, but for most STIS first order medium resolution settings, the sensitivity and standard star flux vary sufficiently slowly with wavelength that this refinement can be neglected.

Detailed procedure

We measured the net count rate as a function of wavelength for each exposure using the standard one-dimensional spectral extraction (x1d or sx1 files) produced by version 2.18 of the CALSTIS software in the STSDAS package. This sums the net counts over a standard height extraction box (7 pixels high for the CCD modes, and 11 pixels high for the MAMA first order modes).

It has been well established that the detected STIS count rates in most modes are affected by time dependent sensitivity (TDS) changes that vary with wavelength (see Stys, Bohlin, & Goudfrooij 2004 and references therein), and count rates in the CCD modes are also subject to charge transfer inefficiency (CTI) losses that vary with time, exposure level, and background level (Goudfrooij et al. 2006). We need to correct the measured net

count rate for these effects to give the sensitivity at a standard reference time and for zero CTI losses. The CALSTIS software, by default, applies corrections for these effects during the conversion from the net count rate to the extracted flux. By simply running the CALSTIS software both with and without the TDS and CTI corrections, we found the appropriate correction vector for each observation, which was then applied to the extracted net count rate vector.

The corrected net count rate vector for each individual observation was then divided by the appropriate WD model flux to yield the sensitivity as a function of wavelength for that observation. The error vector from the CALSTIS extraction was also scaled to provide a corresponding sensitivity error vector for each observation. A multi-node, weighted least squares spline fit was then done to the sensitivity as a function of wavelength. The number of spline nodes used was adjusted to allow the details of the sensitivity curve to be followed while avoiding excessive oscillations in the fit. Where multiple observations exist at a given central wavelength, they were all fit simultaneously, with each point appropriately weighted. This allows measurements made with different exposure times or made using different stars to be directly combined. For example, at the G230M 2095 Å CEN-WAVE (Figure 1), there are two observations of GD 71 and two of G 191-B2B.

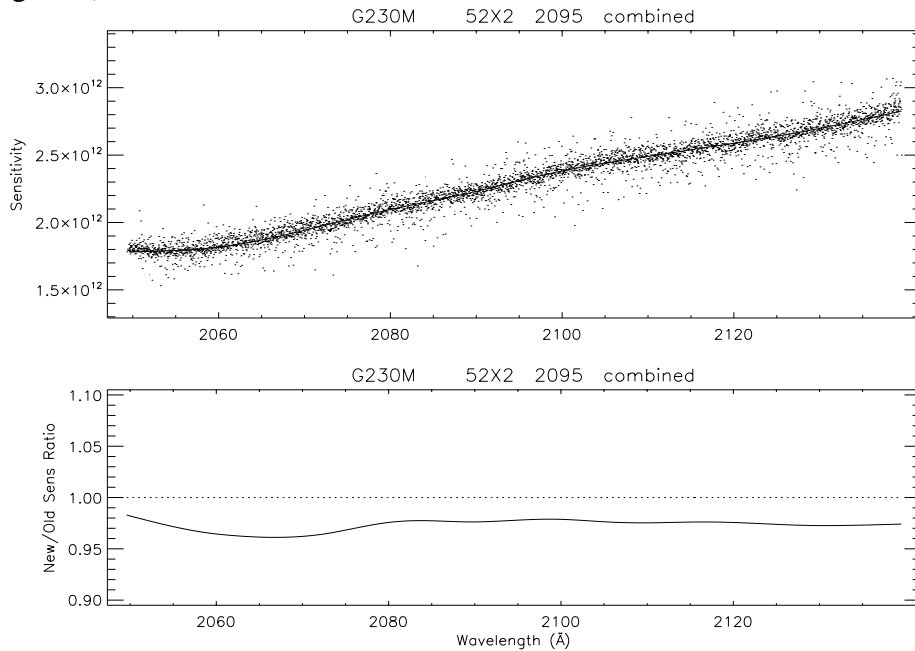


Figure 1: The dots in the upper panel show the pixel-by-pixel sensitivity measurements for all four of the calibration observations of white dwarf standards made at the 2095 Å setting of the G230M grating. The solid line shows the new adopted fit for the measured sensitivity, while the dotted line shows the previous fit used for the generation of the older throughput curves. The units for the sensitivity are (counts/pixel)/(ergs/cm²/Å). The bottom panel shows the ratio of the new to the old sensitivity measurements.

These sensitivity vectors give the (counts/pixel)/(erg/cm²/Å) contained within the default extraction box for observations done with the 52X2 aperture at each detectors reference time and temperature for TDS corrections, and for zero CTI losses. The PHT reference file throughput curves are, however, defined for an infinite extraction box and an infinite aperture. In order to transform the sensitivity vectors into throughput curves, it is necessary to remove the corrections for the finite extraction box, and the aperture throughput, and to divide by the collecting area of HST. When the resulting throughput curve is used to calibrate an actual observation, the tabulated corrections for the particular aperture and extraction box used will be applied. For the standard height extraction box and the 52X2 aperture, these will be the same corrections used to define the throughput curve, and so the accuracy of the extracted fluxes will be unaffected by any errors or uncertainties in the aperture and extraction box height corrections; the fluxes are directly tied to the calibration observations. However, flux values for observations done with other apertures or reduced using other than the default extraction box height will be affected by any differential errors in the tabulated values for these corrections.

Special considerations for individual gratings and wavelengths

Change in G140M MSM Positioning

For the G140M grating settings, the setting of the STIS mode-select-mechanism (MSM) which holds the grating was changed a number of times. During pre-launch testing, the MSM had been set to place G140L and G140M spectra near row 530, but this was too close to the shadow of the FUV-MAMA repeller wire (the NUV-MAMA detector does not have a repeller wire) and in March 1997, shortly after STIS's installation into HST, the grating tilt was changed to put the spectra near row 620 of the detector. In January 1998 an additional small monthly offsetting was added for all MAMA spectroscopic modes to prevent over use of any single portion of the detector. However, an intermittent glow that increases the dark current for the FUV-MAMA detector is strongest in the upper part of the detector, and so in March 1999, the MSM grating tilts for the G140M and G140L detectors were changed again, this time to place first order spectra near row 400 – below the repeller wire and in a part of the detector with significantly lower dark current. It is clear that a separate sensitivity calibration is required for the upper and lower positions. (Note that for the low dispersion G140L grating there are calibration spectra at enough positions along the slit to derive a low order flat field or L-flat, that takes into account most of the sensitivity differences between the two positions; for G140M the large number of central wavelength settings makes such an approach less practical). Unfortunately, at most central wavelengths, GD 71 has been observed only near row 600 and G 191-B2B only near row 400, making it difficult to disentangle vignetting differences at the two positions from differential errors in the model stellar spectra or from inadequacies in the treatment of time dependent sensitivity changes in STIS. This is complicated by the significantly

lower signal-to-noise and the larger number of unmodeled absorption lines in the G 191-B2B spectra. The 1420 Å setting of the G140M provides a good example of these issues. For the upper position we have a single observation of GD 71 (Figure 2), while at the lower position there are two observations of G 191-B2B at this setting (Figure 3), although one of these is at very low S/N. In this case, the other G 191-B2B observation is of sufficiently high S/N to reveal a substantial number of absorption features that are not included in the model spectrum. The obvious lines were masked out of our fit, but at a number of other central wavelengths, the S/N is too low to identify such lines, and this may affect the sensitivity fit by a few percent.

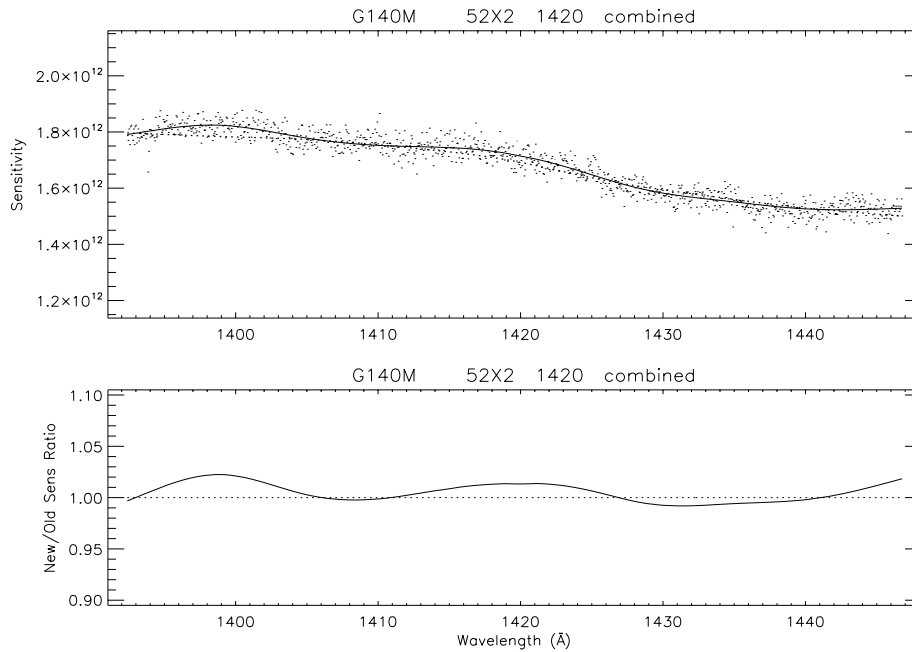


Figure 2: Sensitivity measurements for the G140M 1420 Å setting at the “above-the-repeller-wire” grating position that was in use between March 1997 and February 1999 are based on a single observation of GD 71. Line styles and formatting of this figure are as in Figure 1.

Uncertainties near Lyman- α .

The region near Lyman- α presents special difficulties, as this is the region where the detailed WD model spectra are most likely to be in error. The ratio of the G140M observations of GD 71 and G 191-B2B at the 1222 Å setting to the model spectra cannot be made consistent with the same sensitivity function. The modeled Lyman- α line in GD 71 is too wide relative to that of G 191-B2B to be consistent with the observations, regardless of what assumptions are made about the G140M line spread function. While this may in part be due to the different MSM settings used for the observations of these two stars, it may also be that the model spectra do not accurately reproduce the actual line profile. To avoid these uncertainties, all wavelengths between 1205 and 1240 Å were excluded from the fit

and only 4 spline nodes were used in the fit. This smoothly interpolates the sensitivity curve over the region of the Lyman- α line, but may result in relative flux errors of order 5%.

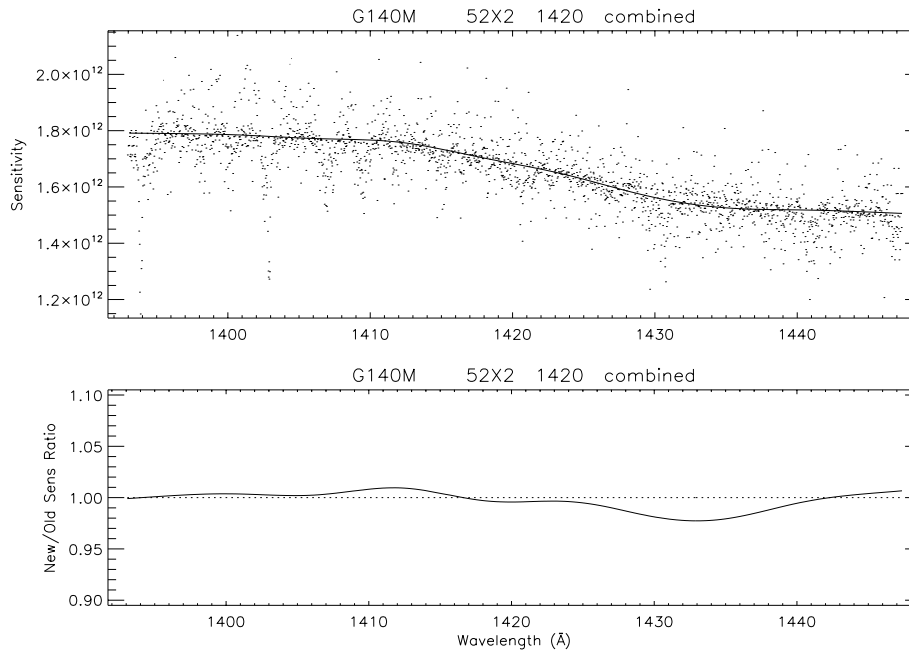


Figure 3: Sensitivity measurements for the G140M 1420 Å setting at the “below-the-repeller-wire” G140M grating position that was the standard position from March 1999 onward, are based on two observations of G 191-B2B (one with a median S/N = 93, and the other with S/N=16). The adopted fit was done using a weighted least-squares fit to the combined data. While the obvious absorption lines were masked out of this fit for the sensitivity, the large number of lines adds considerable uncertainty to the sensitivity measurement. Line styles and formatting are as in Figure 1.

Similar, but more modest caveats apply to some G430M settings where the G 191-B2B spectrum contains H β and other hydrogen lines. In these cases, retaining most wavelengths affected by the lines, results in a reasonable fit, but changes to these lines in the model spectrum might affect the fit at the 1 to 2% level.

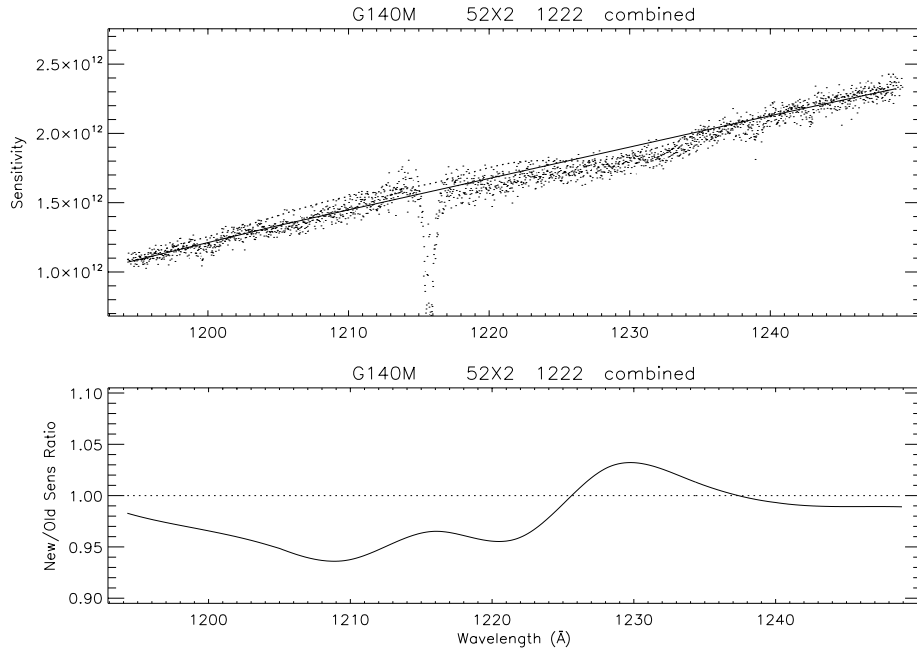


Figure 4: Sensitivity measurements for the G140M 1222 Å setting at the “above-the-repeller-wire” position are based on two observations of GD 71. Because of uncertainties in the modeling of the Lyman- α line, we have interpolated the sensitivity curve smoothly over the uncertain region of the spectrum. Line styles and formatting are as in Figure 1.

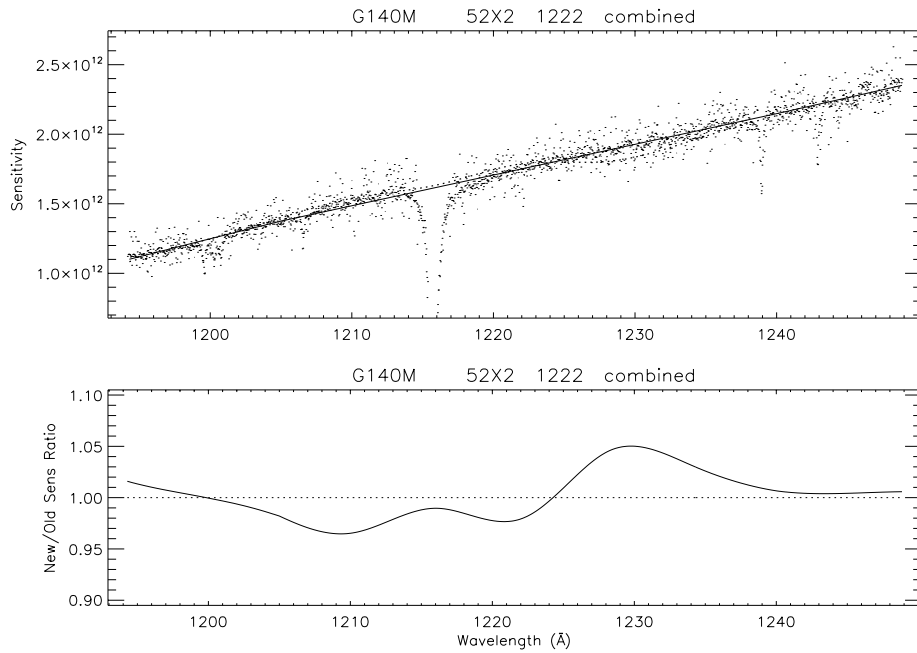


Figure 5: Sensitivity measurements for the G140M 1222 Å setting at the “below-the-repeller-wire” G140M grating position are based on two observations of G 191-B2B. Line styles and formatting are as in Figure 1.

Defringing of G750M spectra

G750M spectra at wavelengths larger than 7000 Å are affected by fringing in the CCD substrate (Walsh et al. 1997). Since the fringe pattern depends on the placement of the spectrum on the detector, it is not appropriate to include the fringing correction in the tabulated throughput curve. Because of the large tilt of G750M spectra, the STScI provided tasks for defringing G750M spectra (Goudfrooij et al. 1997) were only designed to work with 2D rectified files and are not easily used for correcting 1D spectral extractions. To defringe these data we performed simple 1D spectral extractions of tungsten lamp spectra done with the 0.3X0.09 aperture, and then divided the fringe flat spectrum by a 3 node spline fit to itself to remove any lamp vignetting from the fringe flat (Figure 6), giving a normalized fringe flat.

This normalized fringe spectrum was then divided into the corresponding WD spectrum to produce a defringed net count rate spectrum that was used to determine the sensitivity curve (Figure 7). A more careful alignment of the fringe flat with the observed spectrum would probably further improve the S/N, but this alignment provides adequate fringe removal for our purposes. The new throughput curves for G750M tend to have fewer wiggles than do the previous calibration (e.g., Figure 8). This may be due to the inclusion of better fringing corrections in our analysis.

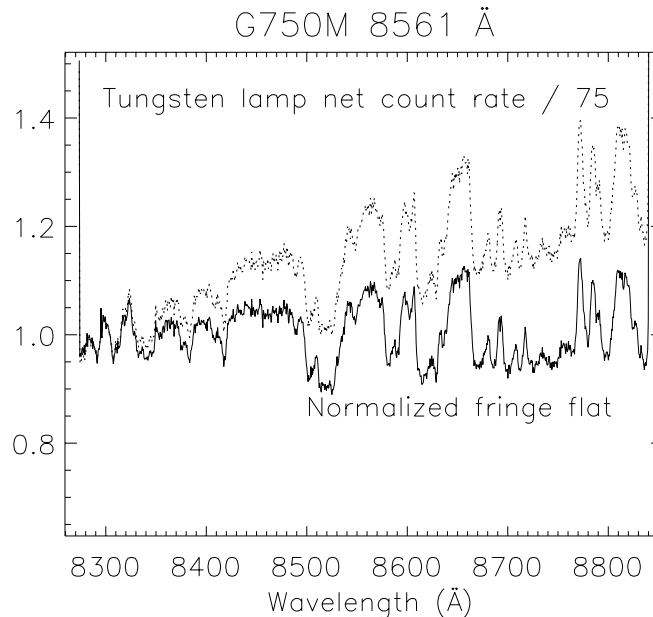


Figure 6: The observed net count rate for a tungsten lamp exposure (data set O6IG080F0) with the G750M at the 8561 Å setting with the 0.3X0.09 aperture is shown by the dotted line. This was divided by a 3 node spline fit to produce a normalized fringe flat (solid line).

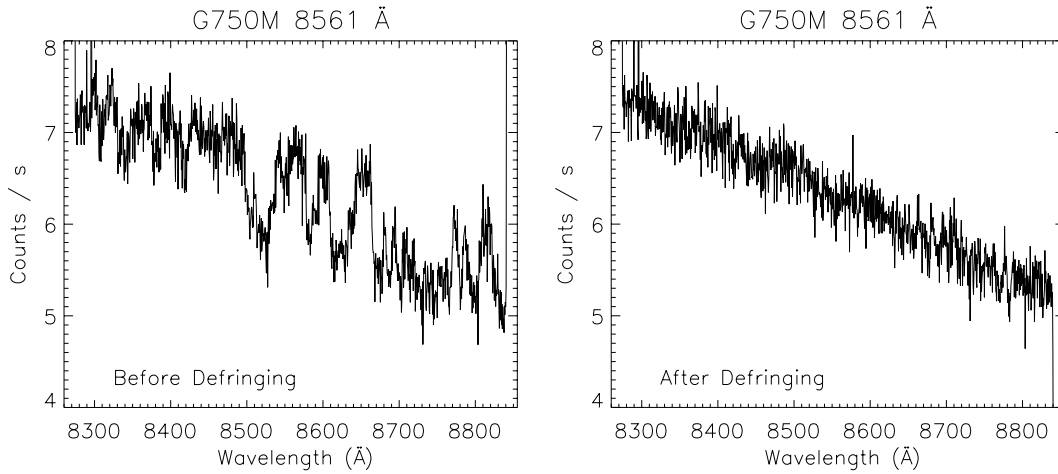


Figure 7: The observed net count rate spectrum for a G750M 8561 Å observation (data set O6IG080E0) of G 191-B2B is shown on the left. Dividing by the normalized fringe flat shown in Figure 6 produces the defringed spectrum shown on the right.

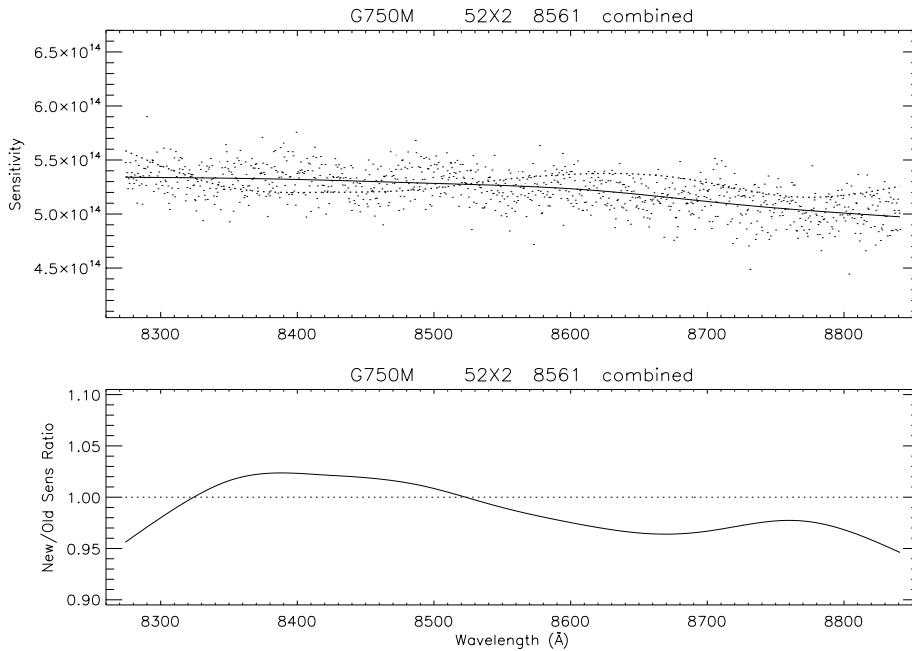


Figure 8: The revised sensitivity measurement for the G750M 8561 Å setting (solid line in upper panel) is based on a fit to the defringed spectrum shown in Figure 7. The previous sensitivity measurement for this grating is shown by the dotted line in the upper panel. Other details of this figure are as in Figure 1.

Missing central wavelengths

For a few rarely used central wavelengths, no observations of primary standard WD stars are available to determine the throughputs. These include G140M 1218 (17 external obser-

vations), and 1400 (7 obs.), G430M 4781 (2 obs.), and G750M 10363 (20 obs.), as well as a few central wavelengths which were never used for external targets (G140M 1387, 1540, 1640; G230M 2600, 2800, 2828; G750M 9286, 9806). For all of these central wavelengths, the throughput curves were left at their previous values.

Accuracy of throughputs

At most wavelengths, the changes from the previous calibration are modest ($< 3\%$), and for observations done at the center of the detector with the 52X2 aperture, the overall flux accuracy should be comparable to the 2% accuracy estimated for low dispersion modes. The G140M calibration is slightly more problematic due to the multiple MSM tilts and uncertainties in the modeling of the Lyman- α profile in WD atmospheres. These uncertainties may cause additional localized flux errors of 2 to 5%.

Variations of throughput with aperture and position

The G430L and G750L gratings contain extra Lyot stops that affect the throughput for different apertures in a complex way (see Proffitt 2006). Separate throughput curves for the grating and the aperture cannot be simply multiplied to give the total throughput. The medium resolution first order gratings lack these Lyot stops and so their throughput should have a simpler behavior as a function of aperture size; however, there are only limited data available to directly test this. For the heavily used 52X0.2 aperture, these limited data suggest that for the CCD medium resolution modes, any systematic throughput discrepancies relative to the 52X2 aperture are no more than 2%, although isolated examples of flux deficits of 3-5% when using the 52X0.2 aperture, (presumably due to slight mis-centering in this aperture), can readily be found. For apertures narrower than the 52X0.2, random throughput variations due to breathing and centering variations probably exceed any systematic errors in the grating or aperture throughputs.

The CCD L-mode and G140L gratings have also been shown to show throughput variations at the few percent level as a function of the target's position along the cross-dispersion direction of the detector (i.e., along the length of the 52" slits). A cursory comparison of some CCD medium resolution (G230MB, G430M, and G750M) sensitivity monitor observations taken using both the standard 52X2 aperture position and the 52X2E1 aperture position defined near the top of the detector, shows that extracted fluxes at the E1 position tend to be systematically low by as much as 5%. For the L-modes, low order flat fields were implemented to correct for such effects. However, for the medium resolution gratings, data comparing throughput as a function of position along the long slit exist only for a limited number of central wavelengths, and it is unclear if these could be interpolated to give low order flat fields suitable for all central wavelengths of the medium resolution gratings. Further work on this issue is needed.

Should STIS be repaired in an HST servicing mission, there are a number of additional calibration observations that would significantly reduce the uncertainties discussed above.

The highest priority would be to observe multiple WD standards at all central wavelengths of the G140M at the current default MSM position (and possibly also at the old “above the repeller-wire” MSM position). Additional observations at various positions along the slit to determine low order flat fields for these gratings, especially for the CCD modes near the E1 positions, and with different slits to check the relative small aperture throughputs with different gratings, would also be useful. However, given the very large number of central wavelength settings, and the limited on-orbit use made of many of these, it is unlikely that time will be available to calibrate all possible CENWAVE , aperture, and slit position combinations to their maximum possible accuracy.

Determining the throughput near Lyman- α would also benefit from observing a flux standard for which the predicted spectral energy distribution near that wavelength is unaffected by uncertainties in the modeling of the Lyman- α line itself. G140L observations (Castanheira et al. 2005) of the DB star GD 358 for example, show that it seems to have little or no hydrogen in its atmosphere, and, at a distance of only about 30 pc, it has a relatively weak interstellar Lyman- α line. While modeling of the spectral energy distribution of this star has not received the attention that the pure hydrogen DA standards have, its very different complement of opacity sources would provide a useful crosscheck on those models.

References

- Bohlin, R. C., Colina, L., & Finley, D. S. 1995, *AJ*, 110, 1316
- Bohlin, R. C., & Gilliland, R. L. 2004, *AJ*, 128, 3053
- Castanheira, B. G., Nitta, A., Kepler, S. O., Winget, D. E., & Koester, D. 2005, *A&A*, 432, 175
- Goudfrooij, P., & Christensen, J. A. 1998, Instrument Science Report STIS 98-29, (Baltimore: STScI)
- Goudfrooij, P., Maíz-Apellániz, J., Brown, T., & Kimble, R. 2006, Instrument Science Report STIS 2006-01, (Baltimore: STScI)
- Proffitt, C. R. 2006, in Proc. 2005 HST Calibration Workshop, eds. A Koekemoer, P. Goudfrooij, & L. Dressel, (Baltimore: STScI), p 199.
- Stys, D. J., Bohlin, R. C., & Goudfrooij, P. 2004, Instrument Science Report STIS 2004-04, (Baltimore: STScI)
- Walsh, J. R., Baum, S. A., Malamuth, E. M., & Goudfrooij, P. 1997, Instrument Science Report STIS 97-16, (Baltimore: STScI)

Appendix

The STIS observations of the WD standard stars GD 71, GD 153, and G 191-B2B that were used to determine the throughputs of the medium resolution first order gratings presented in this report are listed in the following tables. Separate tables are given for the two G140M spectral locations at +3" and -3" that were used for STIS observations with this grating. In each table, the column labeled "n_s" lists the number of spline nodes used in the fit for the sensitivity curve at that central wavelength. The "ypos" column shows the vertical position on the detector where the standard CALSTIS 1D spectral extraction algorithm located the spectral trace. Also listed in these tables are the name of each data set, the target name, the observation date (yyyy-mm-dd), the total exposure time in seconds, and the median signal-to-noise (S/N) of the observation.

Table 1. Observations of WD standards used to determine the sensitivity of G140M modes at the +3'' MSM position. For the 1616 Å position there were no spectra available at the +3'' position, and observations at the -3'' position were substituted.

cenwave	n _s	dataset	target	obsdate	expo time (s)	S/N	ypos
1173	10	o4dd13020	GD 71	1999-03-04	971.00	48.14	620.86
1222	4	o4dd04020	GD 71	1997-11-22	720.00	48.18	614.71
		o4dd13030	GD 71	1999-03-04	720.00	47.64	623.38
1272	4	o4dd04030	GD 71	1997-11-22	720.00	69.42	618.17
		o4dd13040	GD 71	1999-03-04	600.00	62.88	618.91
		o530020f0	G 191-B2B	1999-02-23	120.00	60.82	608.24
1321	10	o4dd04040	GD 71	1997-11-22	600.00	59.34	615.05
		o4dd13050	GD 71	1999-03-04	600.00	58.99	615.17
1371	10	o4dd04050	GD 71	1997-11-22	600.00	51.88	613.33
		o4dd13060	GD 71	1999-03-04	652.00	53.47	615.67
1420	10	o4dd13070	GD 71	1999-03-04	1080.00	59.83	604.86
1470	10	o4dd04060	GD 71	1997-11-22	612.00	38.34	618.79
1518	10	o4dd04070	GD 71	1997-11-22	720.00	34.31	611.77
1550	10	o4dd13080	GD 71	1999-03-04	1080.00	35.30	614.90
1567	10	o4dd04080	GD 71	1997-11-22	720.00	26.97	613.91
1616	10	o4dd14060	GD 71	1999-03-26	2327.00	36.25	385.32
		o5i003070	G 191-B2B	2000-02-28	304.00	27.24	390.11
		o5i003080	G 191-B2B	2000-02-28	1496.00	60.04	390.17
		o6ig060b0	G 191-B2B	2001-11-21	120.00	16.83	382.72
1665	10	o4dd04090	GD 71	1997-11-22	2348.00	31.36	605.81
1714	10	o4dd040a0	GD 71	1997-11-22	2332.00	26.97	614.00

Table 2. Observations of WD standards used to determine the sensitivity of G140M modes at the $-3''$ MSM position. For the 1550 \AA cenwave there were no spectra available at the $-3''$ position, and an observation at the $+3''$ position was substituted.

cenwave	n_s	dataset	target	obsdate	expo time (s)	S/N	ypos
1173	10	o5i003010	G 191-B2B	2000-02-28	600.00	80.92	403.84
		o6ig06010	G 191-B2B	2001-11-21	22.00	15.36	410.93
1222	10	o5i003020	G 191-B2B	2000-02-28	600.00	108.07	405.90
		o6ig06020	G 191-B2B	2001-11-21	15.00	17.50	410.99
1272	4	o530020k0	G 191-B2B	1999-02-23	120.00	60.57	389.90
		o6ig06030	G 191-B2B	2001-11-21	12.00	19.10	403.71
1321	4	o5i003030	G 191-B2B	2000-02-28	395.00	99.95	403.06
		o5i003040	G 191-B2B	2000-02-28	205.00	72.48	403.13
		o6ig06040	G 191-B2B	2001-11-21	12.00	17.62	403.33
1371	10	o6ig06060	G 191-B2B	2001-11-21	4.00	8.80	412.75
		o6ig06070	G 191-B2B	2001-11-21	16.00	17.52	412.92
1420	10	o5i003050	G 191-B2B	2000-02-28	600.00	92.27	404.65
		o6ig06080	G 191-B2B	2001-11-21	20.00	16.77	403.01
1470	10	o4dd14030	GD 71	1999-03-26	600.00	37.14	408.81
		o6ig06050	G 191-B2B	2001-11-21	30.00	17.18	410.31
1518	10	o4dd14040	GD 71	1999-03-26	643.00	31.57	391.13
		o5i003060	G 191-B2B	2000-02-28	600.00	63.67	396.32
		o6ig06090	G 191-B2B	2001-11-21	45.00	17.22	389.78
1550	10	o4dd13080	GD 71	1999-03-04	1080.00	35.30	614.90
1567	6	o4dd14050	GD 71	1999-03-26	720.00	26.15	390.10
		o6ig060a0	G 191-B2B	2001-11-21	70.00	16.67	388.75
1616	6	o4dd14060	GD 71	1999-03-26	2327.00	36.25	385.32
		o5i003070	G 191-B2B	2000-02-28	304.00	27.24	390.11
		o5i003080	G 191-B2B	2000-02-28	1496.00	60.04	390.17
		o6ig060b0	G 191-B2B	2001-11-21	120.00	16.83	382.72
1665	10	o6ig060c0	G 191-B2B	2001-11-21	165.00	16.44	384.71
1714	10	o4dd14020	GD 71	1999-03-26	2086.00	24.91	386.64
		o5i003090	G 191-B2B	2000-02-28	1111.00	37.35	401.98
		o5i0030a0	G 191-B2B	2000-02-28	826.70	32.35	402.00
		o6ig060d0	G 191-B2B	2001-11-21	240.00	16.94	388.80

Table 3. The WD observations used for the calibration of the G230M throughput.

cenwave	n_s	dataset	target	obsdate	expo time (s)	S/N	ypos
1687	6	o4dd10020	GD 71	1999-01-08	2121.00	28.21	515.29
		o5i004010	G 191-B2B	2000-03-04	2520.00	63.75	505.47
		o6ig060e0	G 191-B2B	2001-11-21	180.00	16.89	513.46
		o3zx09ebq	GD 153	1997-05-27	2500.00	27.13	503.35
1769	6	o4dd01020	GD 71	1997-11-10	2096.00	34.55	509.55
		o5i004020	G 191-B2B	2000-03-04	2880.00	83.40	510.15
		o6ig060f0	G 191-B2B	2001-11-21	75.00	13.30	514.59
1851	6	o4dd01030	GD 71	1997-11-10	2338.00	42.60	512.64
		o4dd01030	GD 71	1997-11-10	2338.00	42.60	512.64
		o4dd10040	GD 71	1999-01-08	2536.00	44.67	505.79
		o6ig060g0	G 191-B2B	2001-11-21	60.00	13.92	511.25
		o43j04eeq	GD 153	1997-07-21	550.00	18.91	504.75
1884	6	o4dd11090	GD 71	1999-03-02	2357.00	45.70	509.31
1933	6	o4dd01040	GD 71	1997-11-10	2382.00	47.70	517.66
		o4dd10050	GD 71	1999-01-09	2536.00	49.79	518.16
		o5i004030	G 191-B2B	2000-03-04	2880.00	105.97	513.75
		o6ig060h0	G 191-B2B	2001-11-21	50.00	13.97	518.11
2014	6	o4dd01050	GD 71	1997-11-10	2382.00	50.22	511.54
		o4dd10060	GD 71	1999-01-09	2401.00	50.95	510.43
		o6ig060i0	G 191-B2B	2001-11-21	45.00	13.81	509.73
2095	6	o4dd01060	GD 71	1997-11-10	2382.00	55.39	509.97
		o4dd11040	GD 71	1999-03-01	2492.00	57.05	503.31
		o5i004040	G 191-B2B	2000-03-04	2880.00	120.37	505.81
		o6ig060j0	G 191-B2B	2001-11-21	60.00	17.47	506.90
2176	6	o4dd02030	GD 71	1997-11-23	1000.00	38.53	508.22
		o4dd11030	GD 71	1999-03-01	1526.00	47.72	507.79
		o6ig060k0	G 191-B2B	2001-11-21	32.00	13.70	512.68
2257	6	o4dd02040	GD 71	1997-11-23	1136.00	41.07	514.13
		o5i005010	G 191-B2B	2000-02-28	1000.00	77.22	504.84
		o6ig060l0	G 191-B2B	2001-11-21	35.00	14.35	510.05
2338	6	o4dd11050	GD 71	1999-03-01	1200.00	40.91	513.80

Instrument Science Report STIS 2006-04

cenwave	n _s	dataset	target	obsdate	expo time (s)	S/N	ypos
		o6ig060m0	G 191-B2B	2001-11-21	40.00	14.85	510.88
		o3zx09ejq	GD 153	1997-05-27	975.00	33.01	499.34
2419	6	o4dd02050	GD 71	1997-11-23	1000.00	35.90	509.83
		o4dd11060	GD 71	1999-03-01	1016.00	36.17	509.45
		o5i005020	G 191-B2B	2000-02-28	1090.00	74.19	509.49
		o6ig060n0	G 191-B2B	2001-11-21	40.00	14.24	507.20
2499	6	o4dd02060	GD 71	1997-11-23	1136.00	36.55	510.05
		o4dd11070	GD 71	1999-03-01	1200.00	37.52	511.01
		o6ig060o0	G 191-B2B	2001-11-21	45.00	14.39	509.01
2579	6	o4dd02070	GD 71	1997-11-23	1000.00	32.15	508.38
		o4dd11080	GD 71	1999-03-01	972.00	31.65	508.32
		o5i005030	G 191-B2B	2000-02-28	1200.00	69.72	509.99
		o6ig060p0	G 191-B2B	2001-11-21	50.00	14.19	508.44
2659	6	o4dd02080	GD 71	1997-11-23	1139.00	32.14	514.05
		o6ig060q0	G 191-B2B	2001-11-21	55.00	13.98	511.77
		o43j05euq	GD 153	1997-07-19	585.60	20.88	488.95
2739	6	o4dd02020	GD 71	1997-11-23	1200.00	32.50	495.80
		o5i005040	G 191-B2B	2000-02-28	1200.00	64.15	508.44
		o6ig060r0	G 191-B2B	2001-11-21	60.00	14.35	503.04
2818	10	o4dd03030	GD 71	1998-01-04	2328.00	42.80	506.63
		o6ig060s0	G 191-B2B	2001-11-21	66.00	14.19	515.07
2898	6	o4dd03040	GD 71	1998-01-04	2382.00	38.97	505.70
		o5i005050	G 191-B2B	2000-02-28	2880.00	84.28	516.01
		o6ig060t0	G 191-B2B	2001-11-21	80.00	14.07	505.75
2977	6	o4dd10030	GD 71	1999-01-08	2492.00	34.63	506.28
		o6ig060u0	G 191-B2B	2001-11-21	110.00	14.24	505.36
		o3zx09enq	GD 153	1997-05-27	2705.00	31.18	487.49
3055	6	o4dd03050	GD 71	1998-01-04	2382.00	27.30	505.50
		o5i005060	G 191-B2B	2000-02-28	2880.00	59.64	514.82
		o6ig060v0	G 191-B2B	2001-11-21	155.00	13.80	506.91

Table 4. The WD observations used for the sensitivity calibration of the G230MB grating.

cenwave	n_s	dataset	target	obsdate	expo time (s)	S/N	ypos
1713	6	o5i006010	G 191-B2B	2000-02-27	800.00	32.04	511.83
		o6ig07030	G 191-B2B	2001-09-27	1200.00	38.59	510.69
1854	6	o6ig07040	G 191-B2B	2001-09-27	840.00	53.50	510.19
1995	6	o5i006020	G 191-B2B	2000-02-27	402.00	48.67	513.82
		o6ig070b0	G 191-B2B	2001-09-27	380.00	45.79	510.94
2135	6	o6ig070a0	G 191-B2B	2001-09-27	360.00	54.37	512.56
2276	6	o5i006030	G 191-B2B	2000-02-27	480.00	76.08	510.47
		o6ig07080	G 191-B2B	2001-09-27	280.00	55.73	506.88
2416	15	o6ig07090	G 191-B2B	2001-09-27	280.00	54.84	509.66
2557	6	o5i006040	G 191-B2B	2000-02-27	480.00	71.41	512.48
		o6ig07060	G 191-B2B	2001-09-27	300.00	54.48	508.77
2697	6	o6ig07050	G 191-B2B	2001-09-27	300.00	52.65	512.73
2794	6	o6ig070e0	G 191-B2B	2001-09-27	300.00	49.44	510.19
2836	15	o5i006050	G 191-B2B	2000-02-27	480.00	69.93	509.21
		o5i006060	G 191-B2B	2000-02-27	480.00	70.01	509.22
		o6ig070f0	G 191-B2B	2001-09-27	300.00	53.30	506.82
		o6ig100c0	G 191-B2B	2002-04-22	150.00	35.73	504.21
2976	15	o6ig070g0	G 191-B2B	2001-09-27	220.00	47.81	513.29
3115	6	o5i006070	G 191-B2B	2000-02-27	480.00	79.09	508.33
		o6ig070h0	G 191-B2B	2001-09-27	200.00	48.08	508.22

Table 5. The WD observations used for the sensitivity calibration of the G430M grating.

cenwave	n_s	dataset	target	obsdate	expo time (s)	S/N	ypos
3165	6	o5i007010	G 191-B2B	2000-02-28	400.00	121.40	516.50
		o6ig070i0	G 191-B2B	2001-09-28	120.00	63.39	515.35
3305	6	o6ig070c0	G 191-B2B	2001-09-27	80.00	50.41	520.25
3423	6	o5i007020	G 191-B2B	2000-02-28	400.00	115.01	515.38
		o6ig070j0	G 191-B2B	2001-09-28	120.00	59.83	513.86
3680	6	o6ig070k0	G 191-B2B	2001-09-28	120.00	61.85	514.65
3843	6	o6ig07070	G 191-B2B	2001-09-27	80.00	54.78	514.48
3936	6	o5i007030	G 191-B2B	2000-02-28	438.00	140.86	515.67
		o6ig08020	G 191-B2B	2001-09-24	60.00	47.99	514.95
4194	6	o6ig08030	G 191-B2B	2001-09-24	70.00	50.83	515.52
4451	6	o5i007040	G 191-B2B	2000-02-28	480.00	135.73	515.82
		o6ig070m0	G 191-B2B	2001-09-28	80.00	51.87	517.01
4706	6	o6ig070d0	G 191-B2B	2001-09-27	90.00	49.84	511.17
4961	6	o5i007050	G 191-B2B	2000-02-28	480.00	119.55	516.00
		o6ig07020	G 191-B2B	2001-09-27	100.00	50.67	516.21
5093	6	o6ig08010	G 191-B2B	2001-09-24	100.00	50.54	515.81
5216	6	o6ig070l0	G 191-B2B	2001-09-28	120.00	52.50	531.86
5471	6	o5i007060	G 191-B2B	2000-02-28	480.00	95.63	511.16
		o6ig070n0	G 191-B2B	2001-09-28	150.00	50.05	510.12

Table 6. The WD observations used for the sensitivity calibration of the G750M grating.

cenwave	n _s	dataset	target	obsdate	expo time (s)	S/N	ypos
5734	6	o5i008010	G 191-B2B	2000-01-30	480.00	140.95	515.90
		o6ig08040	G 191-B2B	2001-09-24	70.00	49.70	515.25
6094	6	o6ig08050	G 191-B2B	2001-09-24	80.00	50.45	489.70
6252	6	o6ig08060	G 191-B2B	2001-09-24	90.00	53.09	515.90
6581	6	o6ig07010	G 191-B2B	2001-09-27	120.00	58.48	511.76
6768	6	o5i008020	G 191-B2B	2000-01-30	480.00	119.24	516.32
		o6ig08070	G 191-B2B	2001-09-24	100.00	50.89	515.68
7283	6	o6ig08080	G 191-B2B	2001-09-24	140.00	51.67	516.80
7795	6	o5i008030	G 191-B2B	2000-01-30	480.00	79.08	513.04
		o6ig080a0	G 191-B2B	2001-09-24	210.00	49.56	509.51
8311	6	o6ig080c0	G 191-B2B	2001-09-24	360.00	46.48	512.45
8561	6	o6ig080e0	G 191-B2B	2001-09-24	400.00	45.63	512.08
8825	6	o5i008050	G 191-B2B	2000-01-30	480.00	48.77	514.28
9336	6	o6ig080g0	G 191-B2B	2001-09-25	540.00	40.85	508.09
9851	6	o5i008070	G 191-B2B	2000-01-30	480.00	22.69	511.42
		o6ig080i0	G 191-B2B	2001-09-25	690.00	26.91	513.05